Dynamics and Controls

Purpose

The purpose of the dynamics and controls team can be summarized by the following points:

- Size the tail and control surfaces
- Characterize aircraft handling and dynamic response
- Determine feedback control systems

Tail Sizing

Class 1 Tail Sizing

The first iteration of tail size was determined through the use of a method described by Jan Roskam in his book "Airplane Design" [1]. Roskam refers to this preliminary sizing technique as the "Class I Method for Empennage Sizing and Disposition and For Control Surface Sizing and Disposition." A method summary is given below:

1) Decide on tail configuration
2) Determine distance from aircraft wing to tail
3) Determine tail surface area
4) Determine tail geometry
5) Determine control surface sizing and disposition

Step 1: The tail configuration chosen for their aircraft was a conventional twin-boom tail with rectangular planform surfaces for the horizontal and vertical stabilizers. This decision was made early in the design phase while selecting possible aircraft configurations. It was decided that the twin-boom design allowed for simplest design and manufacture of the aircraft.

Step 2: The distance from the aircraft center of gravity to the aerodynamic center of the horizontal and vertical stabilizers was determined to be 2.7 feet. This was determined by finding the largest possible tail boom length while allowing the aircraft to be disassembled and fit inside of the provided storage container – a requirement of the RFP.

Step 3: The tail surface area was determined through Equation 1:

[1]

$$S_h = \frac{V_h S \bar{c}}{X_h} = \frac{(0.47)(5.14ft^2)(0.88ft)}{(2.7ft)} = 0.78ft^2$$
$$Sv = \frac{V_v S b}{X_v} = \frac{(0.036)(5.14ft^2)(5.87ft)}{(2.7ft)} = 0.406ft^2$$

$$where\ S_h = horizontal\ tail\ area$$
$$V_h = horizontal\ tail\ volume\ coefficient$$
$$S = wind\ area$$
$$\bar{c} = mean\ wing\ chord$$
$$x_h = horizontal\ tail\ moment\ arm$$
$$V_v = vertical\ tail\ volume\ coefficient$$
$$b = wingspan$$
$$x_v = vertical\ tail\ moment\ arm$$

To elaborate upon this analysis, the wing area, chord and wingspan were determined by the aerodynamics team. The moment arms were determined in the previous Class I sizing step. The tail volume coefficients were determined through the use of historical data pertaining to homebuilt airplanes. This historical data is shown below in Table 1. Note that the volume coefficients used in Equation 1 were the average value of the volume coefficients found in the presented historical data.

Table 1: Historical data pertaining to homebuilt airplanes [1]

	wing area ft^2	wing chord ft	horizontal tail area ft^2	Se/Sh	Xh ft	Vh	elevator root chord frac Ch	elevator tip chord frac Ch
PIK-21	76.4	4.5	10.4	0.45	10.1	0.3	0.45	0.45
RD-03C	119	4.3	22.2	0.33	11.3	0.49	0.47	0.32
CP-750	118	3.82	23.5	0.51	12.6	0.66	0.55	0.47
CP-90	104	3.81	22.9	0.5	11.8	0.66	0.56	0.38
P-50R	80.7	3.74	13.4	0.52	10.6	0.47	0.5	0.55
P-70S	77.5	4.1	14.5	0.6	9.68	0.44	0.6	0.6
Aerosport Aerocar	80.7	3.77	15.4	0.48	10.6	0.54	0.48	0.48
Micro-Imp	81	3	11.7	0.25	6.27	0.3	0.28	0.33
SA-III	112	4.5	16.5	0.46	10.9	0.36	0.46	0.46
300 Ord-Bume	130	4.37	25.5	0.43	13.2	0.59	0.43	0.43
OH-4B	125	5.25	25.4	0.49	11.1	0.43	0.49	0.49
Petrel	135	4.54	26	0.52	12.2	0.52	0.52	0.52
Bade BD-8	96.7	5	19.4	0.14	7.64	0.31	0.17	0.17
AVERAGE	102.77	4.21	18.98	0.44	10.61	0.47	0.46	0.43

	wing area ft^2	wing span ft	Vertical tail area ft^2	Sr/Sv	Xv ft	Vv	rudder root chord frac Cv	ruddet tip chord frac Cv	Sa/S	aileron Span Location (in) frac b/2	aileron Span Location (out) frac b/2	Aileron Chord (in) frac Cw	Aileron Chord (out) frac Cw
PIK-21	76.4	17	3.49	0.33	10.5	0.028	0.24	0.49	0.13	0	1	0.13	0.13
RD-03C	119	29.7	8.35	0.3	12.5	0.031	0.38	0.32	0.063	0.63	0.93	0.22	0.24
CP-750	118	26.4	9.49	0.55	12.9	0.039	0.5	0.64	0.077	0.44	0.96	0.19	0.14
CP-90	104	23.6	7.64	0.5	11.9	0.037	0.47	0.54	0.092	0.42	0.91	0.22	0.18
P-50R	80.7	20.3	11.3	0.42	10.4	0.072	0.84	0.61	0.067	0.6	0.98	0.24	0.22
P-70S	77.5	19.4	4.36	0.67	10.5	0.031	0.59	0.76	0.082	0.52	0.88	0.2	0.2
Aerosport Aerocar	80.7	23.3	6.86	0.38	10.6	0.04	0.34	0.44	0.08	0.54	0.97	0.19	0.19
Micro-Imp	81	27	7.15	0.31	6.27	0.02	0.33	0.43	0.14	0.07	0.95	0.16	0.16
SA-III	112	25	7.53	0.44	10.6	0.028	0.35	0.68	0.13	0.55	1	0.26	0.26
300 Ord-Bume	130	30	16.5	0.31	13.2	0.055	0.27	0.43	0.085	0.6	0.95	0.29	0.29
OH-4B	125	25	6.73	0.71	12.5	0.027	0.57	1	0.11	0.35	0.91	0.2	0.2
Petrel	135	30	11.7	0.35	11.4	0.033	0.32	0.57	0.097	0.62	0.98	0.26	0.26
Bade BD-8	96.7	19.3	6.89	0.24	8.65	0.032	0.2	0.34	0.083	0.53	0.92	0.22	0.22
AVERAGE	102.77	24.31	8.31	0.42	10.92	0.04	0.42	0.56	0.10	0.45	0.95	0.21	0.21

Step 4: Tail geometry was selected with this assistance of additional historical data, illustrated in Table 2.

Table 2: Historical data pertaining to homebuilt airplane tail geometry [1]

Homebuilt Horizontal Tail				
dihedral angle	incidence angle	aspect ratio	sweep angle	taper ratio
deg	deg		deg	
+5 - (-10)	0	1.8 - 4.5	0 - 20	0.29 - 1.0
Homebuilt Vertical Tail				
dihedral angle	incidence angle	aspect ratio	sweep angle	taper ratio
deg	deg		deg	
90	0	0.4 - 1.4	0 - 47	0.26 - 0.71

The aspect ratio of the horizontal stabilizer was determined by finding the mean value for aspect ratio presented by the historical data in Table 2. This corresponded to an aspect ratio of 3.15. As discussed, since the horizontal tail has a rectangular planform area, this yielded a horizontal tailspan of 1.56 feet and a chord of 0.5 feet.

Recall that the vertical tail is composed to 2 vertical surfaces – one connected to each tail boom. For simplicity and ease of manufacture, the vertical tail chord was constrained to be the same as the horizontal tail chord. This constraint yielded a vertical tail chord of 0.5 feet and a vertical tail height of 0.41 feet. This yielded a vertical tail aspect ratio of 0.82, well within the bounds for typical vertical tail aspect ratio presented by historical data in Table 2.

The taper ratio was determined to be 1, the dihedral angle was determined to be 0 degrees, and the incidence angle was determined to be 0 degrees. These decisions were made to keep the tail design and manufacture simple.

Step 5: The control surface sizes and disposition were determined using the historical data presented in Table 1. More specifically, the averages values were taken; the results are shown below.

Table 3: Control Surface Sizing

Historical Control Surface Sizes				
Elevator chord	Rudder Chord	Aileron Chord	Aileron Location (in)	Aileron Location (out)
frac Ch	frac Cv	frac Cw	frac b/2	frac b/2
0.45	0.49	0.21	0.45	0.95

The final results from the Class I sizing method are illustrated below:

Table 4: Results from Class I sizing method

resulting tail dimension				
horizontal tail span	horizontal tail chord	vertical tail chord	vertical tail height	
ft	ft	ft	ft	
1.56	0.50	0.50	0.41	
resulting control surface dimenstions				
Elevator chord	Rudder Chord	Aileron Chord	Aileron Location (in)	Aileron Location (out)
ft	ft	ft	ft	ft
0.22	0.24	0.18	1.33	2.79

Horizontal Tail X-Plot

The Class I sizing method allowed for a first iteration sizing of the tail. This allowed for an improved CAD model and an improved confidence on the location of center of gravity for the aircraft. However, the Class I sizing method relies heavily upon historical data. The use of historical data causes issues when the examined historical aircraft have differences in design and mission from our team's aircraft. As such, the method of "X-plots" was used to fine-tune the tail sizes and produce more confident results.

The longitudinal X-plot refers to the plotting of the aircraft center of gravity and aerodynamic center as a function of horizontal tail surface area. The distance between the aircraft center of gravity and aerodynamic center is commonly referred to as the static margin. For an aircraft to be statically stable, the aircraft center of gravity must be forward for the aerodynamic center – corresponding to a positive static margin. Since this is desirable, the X-plot can be used to examine the static stability of the aircraft as a function of horizontal tail area.

The aircraft aerodynamic center was determined through Equation 2, found in "Airplane Design" by Jan Roskam [1].

[2]

The a.c. leg is calculated with the following equations:

$$\bar{X}_{ac_A} = [\bar{X}_{ac_{wf}} + \{C_{L_{\alpha_h}}(1 - d\varepsilon_h/d\alpha)(S_h/S)\bar{X}_{ac_h} - C_{L_{\alpha_c}}(1 + d\varepsilon_c/d\alpha)\bar{X}_{ac_c}(S_c/S)\}/C_{L_{\alpha_{wf}}}]/F, \quad (11.1)$$

where:

$$F = [1 + \{C_{L_{\alpha_h}}(1 - d\varepsilon_h/d\alpha)(S_h/S) + C_{L_{\alpha_c}}(1 + d\varepsilon_c/d\alpha)(S_c/S)\}/C_{L_{\alpha_{wf}}}] \quad (11.2)$$

For Equation 2: the wing area, wing lift curve slope, and the tail lift curve slope was determined and provided by the aerodynamics team.

The downwash curve slope was determined empirically through the use of Figure 16.12 in “Aircraft Design” by Daniel Raymer. The appropriate figure is shown below.

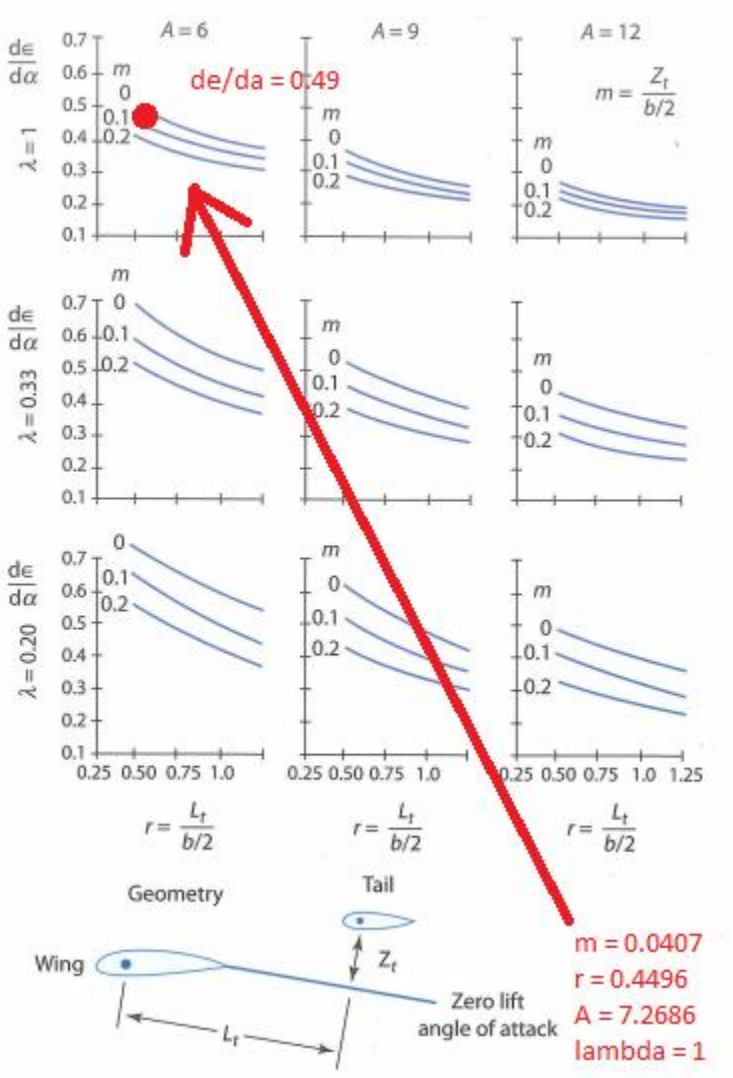

Figure 1: Determination of downwash curve slope using Figure 16.12 in Raymer text [2]

The center of gravity as a function of horizontal tail surface area was determined through the use of the aircraft CAD model maintained by the structures team. More specifically, several tail sizes were specified in the model and the corresponding center of gravity locations were recorded. The data fit to a linear curve, shown below.

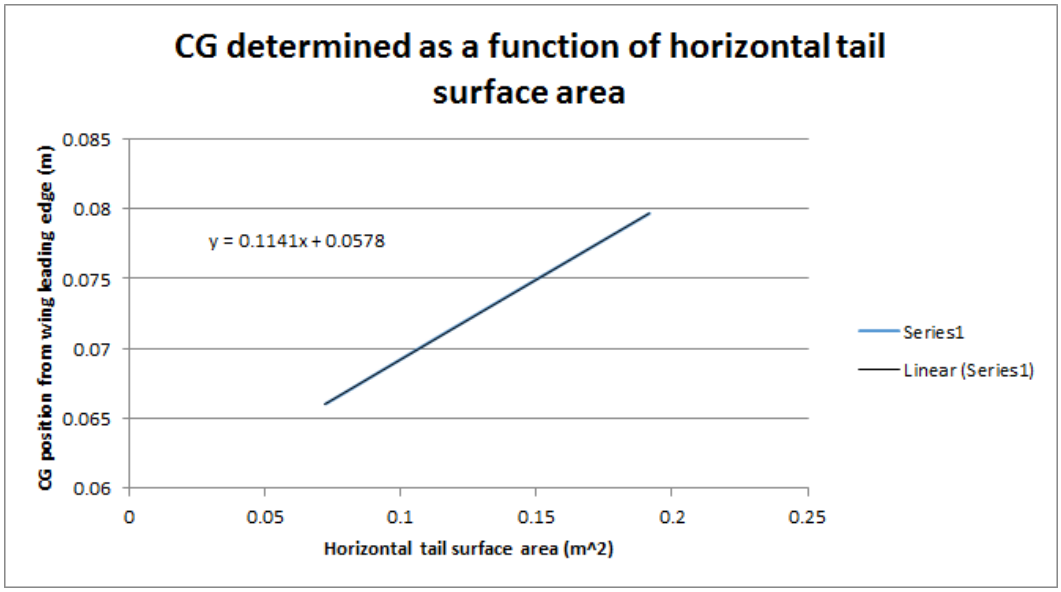

Figure 2: Determination of CG as a function of horizontal tail surface area

With the determination of CG and AC as a function of tail area, the results were plotted and can be found in Figure 3. The tail surface area was iterated from 0 to 2 square feet.

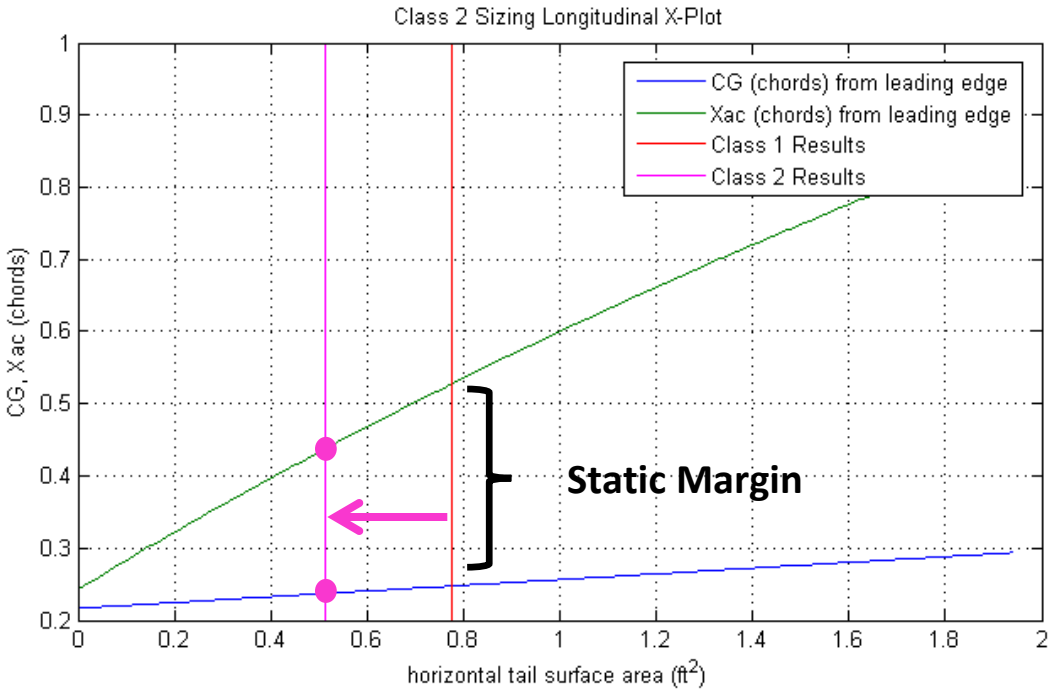

Figure 3: Longitudinal X-plot

From Figure 3, we see that as tail size increases, the center of gravity moves towards the tail of the plane. Similarly, as the tail size increases, the aerodynamic center moves towards the tail of the plane. More importantly, as the tail size increases, the static margin (the distance between the CG and AC) also

increases. As such, Figure 3 illustrates that it is possible to select a specific static margin by specifying the horizontal tail size of the aircraft.

In "Aircraft Design" by Jan Raymer, Raymer specifies that a Cessna 172 has a static margin of 0.19 chords. Typically, commercial airliners have lower static margins – this allows for increased turning performance. However, Raymer concludes that hobby aircraft and personal aircraft have larger static margins to allow for easy and forgiving aircraft handling. As such, our team chose to select a static margin of 0.2 chords. This corresponds to a CG location of 0.24 chords and an AC location of 0.44 chords.

From Figure 3, we see that the tail size determined by the Class I sizing method yields a static margin of 0.28 chords. To achieve the desired static margin of 0.20 chords, the tail size must be reduced slightly from 0.78 square feet to 0.51 square feet. The results of the horizontal tail sizing methods are tabulated and compared in Table 5. The X-plot tail sizing results are the values to be used for aircraft manufacture.

Table 5: Horizontal Tail Sizing Results Comparison

Class 1 sizing - Horizontal Tail			
Area	span	chord	Static Margin
ft^2	ft	ft	
0.78	1.56	0.5	0.28
X-plot sizing - Horizontal Tail			
Area	span	chord	Static Margin
ft^2	ft	ft	
0.51	1.03	0.5	0.2

Vertical Tail X-Plot

Similarly to the horizontal tail X-plot method, an X-plot was generated for the vertical tail to fine-tune the tail size from the size determined by the Class I method. The vertical tail X-plot refers to the plotting of aircraft yawing moment coefficient as a function of vertical tail surface area. More specifically, the yawing moment coefficient describes the response of the aircraft to a sideslip force. With a positive yawing moment coefficient, the aircraft will tend towards yawing into the direction of the sideslip force. Over time, this will reduce the sideslip angle of attack and stabilize the aircraft. This is a desired aircraft characteristic.

The yawing moment coefficient was found using the following sequence of equations. These equations can be found in "Methods for Estimating Stability and Control Derivatives of Conventional Subsonic Airplanes" by Jan Roskam [3].

[3]

$$C_{n_\beta} = C_{n_{\beta_W}} + C_{n_{\beta_B}} + C_{n_{\beta_V}} \qquad (7.15)$$

$$C_{n_{\beta_B}} = -57.3\, K_N\, K_{R_\ell}\, \frac{S_{B_s}}{S}\, \frac{\ell_B}{b} \quad (\text{rad}^{-1}) \qquad (7.16)$$

$$C_{n_{\beta_V}} = -C_{y_{\beta_V}}\, \frac{(\ell_V \cos\alpha + Z_V \sin\alpha)}{b} \quad (\text{rad}^{-1}) \qquad (7.17)$$

$$C_{y_{\beta_V}} = -kC_{L_{\alpha_V}} \left(1 + \frac{d\sigma}{d\beta}\right) \eta_V \frac{S_V}{S} \quad (\text{rad}^{-1}) \qquad (7.4)$$

$$\left(1 + \frac{d\sigma}{d\beta}\right)\eta_V = .724 + 3.06\, \frac{S_V/S}{1 + \cos\Lambda_{c/4}} + .4\, \frac{Z_w}{d} + .009A \qquad (7.5)$$

From this analysis, we see that the yawing moment coefficient requires the following empirical constants: K_N, K_{R_l}, k. Figures A1, A2, and A3 in the appendix illustrate how these constants were obtained through tables provided in the Roskam text.

The X-plot was generated for a tail size from 0 to 0.7 square feet and can be found below.

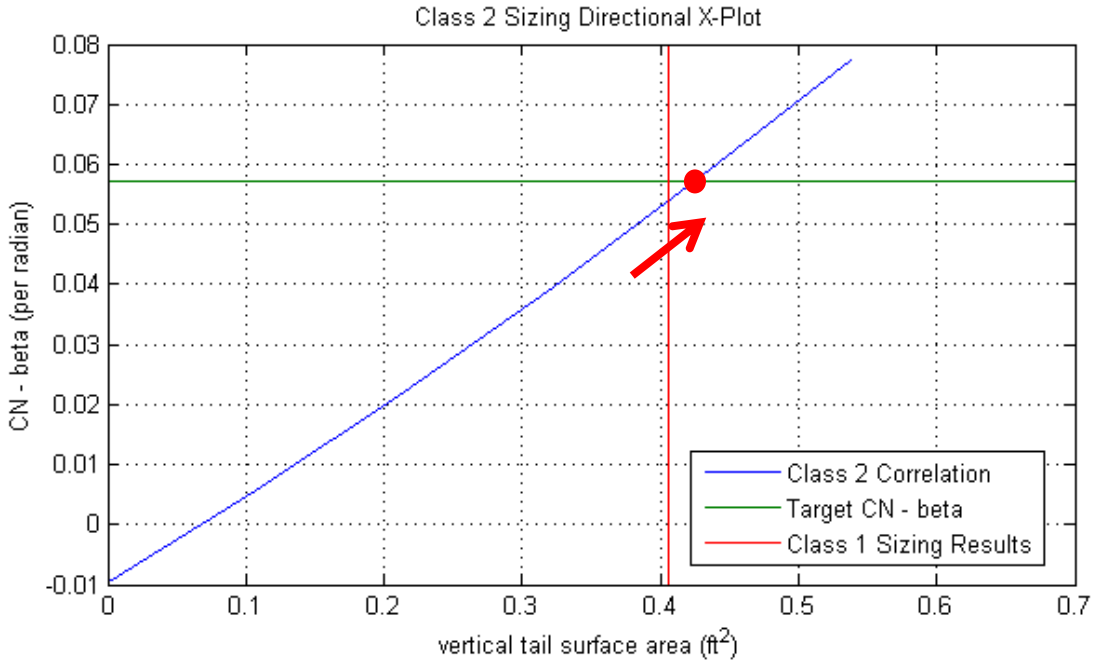

Figure 4: Lateral X-Plot

From Figure 4, we see that without a vertical tail, the yawing moment coefficient is negative – this corresponds to a directionally unstable aircraft. However, as vertical tail size increases, the yawing moment also increases.

Roskam suggests that a directionally stable aircraft have a yawing moment coefficient of approximately 0.0010 per degree. In accordance with this standard, Figure 4 shows that our aircraft requires a vertical tail area of 0.427 square feet. This requires a slight increase in tail size from the Class I analysis. The final results of the vertical tail sizing are tabulated and compared in Table 6. The X-plot tail sizing results are the values to be used for aircraft manufacture.

Table 6: Vertical Tail Sizing Results Comparison

Class 1 sizing - Vertical Tail			
Area	height	chord	Yawing Moment Coefficient
ft^2	ft	ft	per radian
0.427	0.41	0.5	0.053
X-plot sizing - Vertical Tail			
Area	height	chord	Yawing Moment Coefficient
ft^2	ft	ft	per radian
0.406	0.429	0.5	0.057

Dynamic Flying Quality Analysis

Introduction

Flying Quality Levels	
Level 1	Flying qualities clearly adequate for the mission Flight Phase
Level 2	Flying qualities adequate to accomplish the mission Flight Phase, but some increase in pilot workload or degradation in mission effectiveness, or both, exists
Level 3	Flying qualities such that the airplane can be controlled safely, but pilot workload is excessive or mission effectiveness is inadequate, or both. Category A Flight Phases can be terminated safely, and Category B and C Flight Phases can be completed.

Classification	Aircraft Type	Examples
Class I	Small, light airplanes	Light utility, primary trainer, light observation
Class II	Medium-weight, low-to-medium maneuverability	Heavy utility/search and rescue, light or medium transport/cargo/tanker, recon, tactical bomber
Class III	Large, heavy, low-to medium maneuverability	Heavy transport/cargo/tanker, heavy bomber
Class IV	High maneuverability	Fighter/interceptor, attack, tactical recon

	Description	Include in category:
Category A	Those non-terminal flight phases that require rapid maneuvering, precision tracking or precise flight path control.	Air-to-air combat, ground attack, weapon deliver/launch, aerial recovery reconnaissance, in-flight refueling, terrain following, anti-submarine search, close formation flying
Category B	Those non-terminal flight phases that are normally accomplished using gradual maneuvers and without precision tracking, although accurate flight-path control may be required.	Climb, cruise, loiter, in-flight refueling (tanker) descent, emergency descent, emergency deceleration, aerial delivery
Category C	Terminal flight phases are normal accomplished using gradual maneuvers and usually require accurate flight path control.	Takeoff, catapult takeoff, approach, wave-off/go-around, landing

Transfer functions

FlatEarth v9.53 was utilized to characterize the dynamical motion of the designed aircraft. The dynamic model was linearized and the following transfer functions were obtained from the resulting state space.

From input "deltaE(r)" to output "q(r/s)":

$$\frac{-35.24\,s^4 - 174.9\,s^3 - 105.1\,s^2 - 0.004634\,s}{s^5 + 9.748\,s^4 + 44.52\,s^3 + 22.8\,s^2 + 53.75\,s + 0.003176}$$

From input "deltaA(r)" to output "p(r/s)":

$$\frac{107.3\,s^3 + 285.3\,s^2 + 2883\,s - 472.8}{s^4 + 23.48\,s^3 + 124.3\,s^2 + 575.1\,s - 334}$$

From input "deltaR(r)" to output "r(r/s)":

$$\frac{-19.26\,s^3 - 399.8\,s^2 - 84.73\,s - 21.75}{s^4 + 23.48\,s^3 + 124.3\,s^2 + 575.1\,s - 334}$$

From input "deltaR(r)" to output "p(r/s)":

$$\frac{1.646\,s^3 - 14.25\,s^2 - 32.52\,s + 0.357}{s^4 + 11.84\,s^3 + 16.96\,s^2 + 74.61\,s - 5.602}$$

We are primarily interested in these transfer functions as they pertain to how the control surface inputs affect aircraft flight dynamics.

Characteristic equations

From the transfer functions, we note that roll rate and yaw rate output transfer functions share the same denominator. This denominator corresponds to the characteristic polynomial for lateral motion. More specifically, the characteristic polynomial describes the output motion of a system without input. Similarly, the denominator for the pitch rate output transfer function corresponds to the characteristic polynomial for longitudinal motion.

By setting the characteristic polynomial to zero, we obtain the characteristic equation. The roots of the characteristic equation yield information pertaining to the response of the system without input. The following plots illustrate these roots for both the longitudinal and lateral systems. Note that these roots have associated names due to their high significance.

Longitudinal motion characteristic equation:

s^5 + 9.748 s^4 + 44.52 s^3 + 22.8 s^2 + 53.75 s + 0.003176 = 0

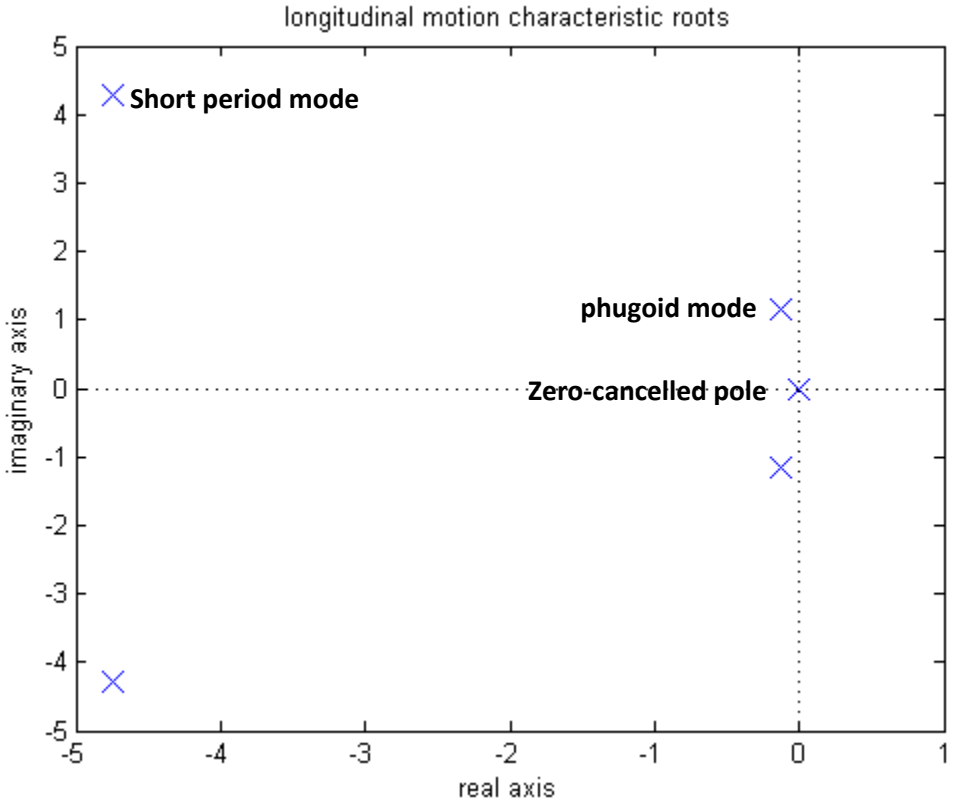

Figure XXX: longitudinal motion characteristic roots

Lateral motion characteristic equation:

s^4 + 23.48 s^3 + 124.3 s^2 + 575.1 s – 334 = 0

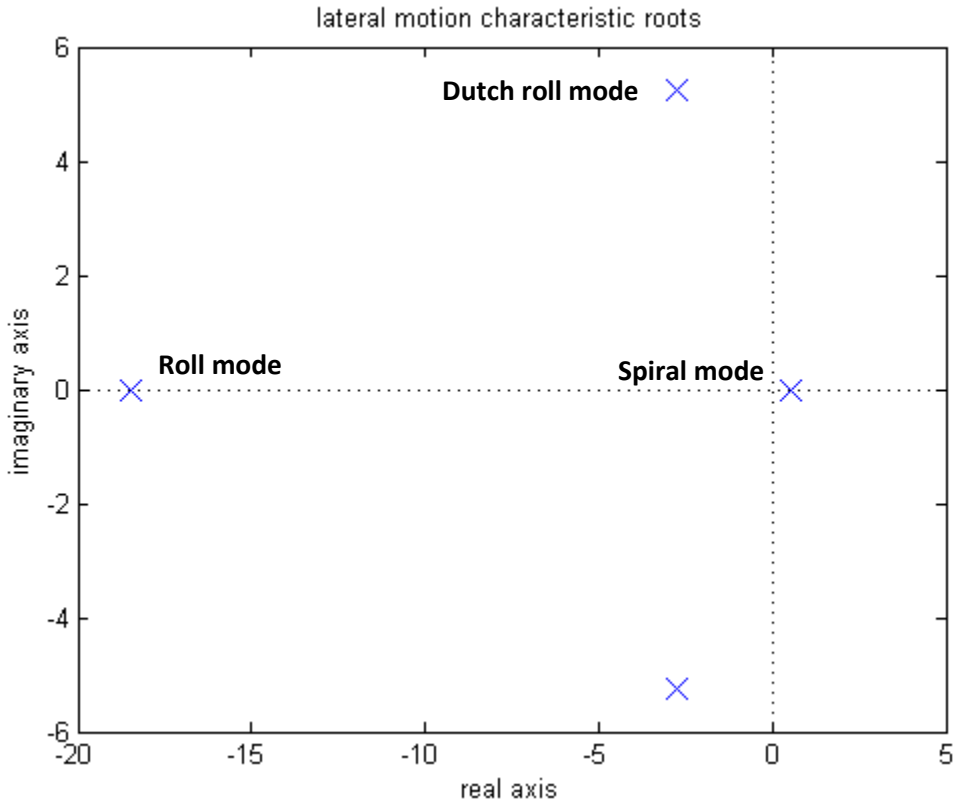

Figure XXX: lateral motion characteristic roots

Table XXX: characteristic roots for various aircraft

	Team 2 Designed Aircraft				
	Longitudinal Open-loop		Lateral Open-loop		
	short period	Phugoid mode	dutch roll	roll mode	spiral
roots	-4.75 +/- 4.27i	-0.13 +/- 1.14i	-2.75 +/- 5.23i	-18.50	0.52
damping ratio	0.74	0.11	0.47	1.00	-1.00
natural frequency (r/s)	6.39	1.15	5.91	18.50	0.52
	MPX5 Test case aircraft				
	Longitudinal Open-loop		Lateral Open-loop		
	short period	Phugoid mode	dutch roll	roll mode	spiral
roots	-6.13 +/- 6.50i	-0.05 +/- 0.59i	-0.92 +/- 3.79i	-15.17	0.19
damping ratio	0.69	0.09	0.24	1.00	-1.00
natural frequency (r/s)	8.94	0.60	3.90	15.17	0.19
	PA_28_161_Warrior Test case aircraft				
	Longitudinal Open-loop		Lateral Open-loop		
	short period	Phugoid mode	dutch roll	roll mode	spiral
roots	-2.90 +/- 4.95i	-0.03 +/- 0.25i	-0.50 +/- 2.59i	-10.92	0.07
damping ratio	0.51	0.10	0.19	1.00	-1.00
natural frequency (r/s)	5.74	0.25	2.64	10.92	0.07

Table XXX illustrates the lateral and longitudinal characteristic roots for three separate aircraft. The first aircraft corresponds to the current aircraft design for Team 2. The MPX5 aircraft represents a UAV designed by Mark Peters for a Masters Thesis in 1996. The Warrior represents a small manned aircraft. The following analysis in this report will include and compare these 3 aircraft.

Phugoid motion

Phugoid motion corresponds to the long-term oscillation of the aircraft in the longitudinal direction. The following figure illustrates this motion.

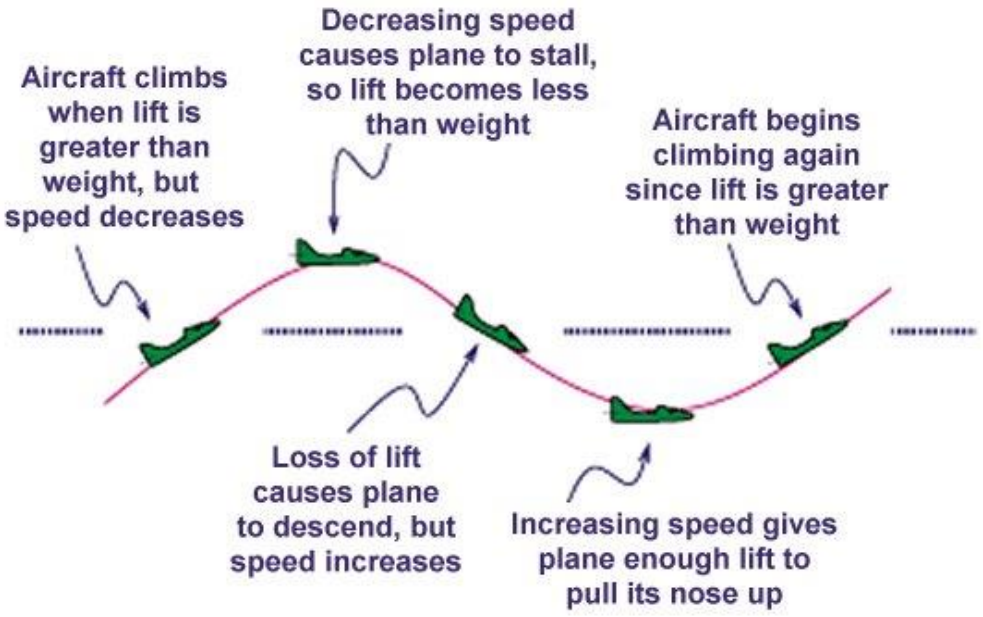

Figure XXX: illustration of long-term phugoidal motion in longitudinal direction

Typically, the period for phugoidal motion is near 30 seconds. It is desirable for this motion to dampen over time and slowly arrest the amplitude of oscillation. The following equation correlates flying quality to the phugoidal damping ratio.

Level 1	equivalent $\zeta_p > 0.04$
Level 2	equivalent $\zeta_p > 0$
Level 3	$T_2 \geq 55$ seconds

$$where\ \zeta_p = phugoid\ mode\ damping\ ratio$$
$$T_2 = time\ to\ double\ amplitude$$

Table XXX: Phugoid mode flying quality

	phugoid mode damping quality	
	phugoid mode damping ratio	Flying quality level
Team 2 aircraft	0.11	1
MPX5 test case	0.09	1
Warrior test case	0.10	1

Table XXX illustrates that the current aircraft design yields an open-loop phugoidal mode damping ratio of 0.11. Since this value is greater than 0.04, the aircraft is best described by level 1 flying quality. This corresponds to a stable and easy-to-control aircraft in this mode.

Short Period Mode

Damping ratio range

The short period mode corresponds to short-term oscillations caused by either changes in control inputs or by gusts of wind. It is desirable to keep the damping ratio within a specified range for this motion. More specifically, if the damping ratio is too low, the oscillation amplitude can be too large. However, if the damping ratio is too large, the control input response can appear sluggish. The following table correlates short-term damping ratio to flying quality.

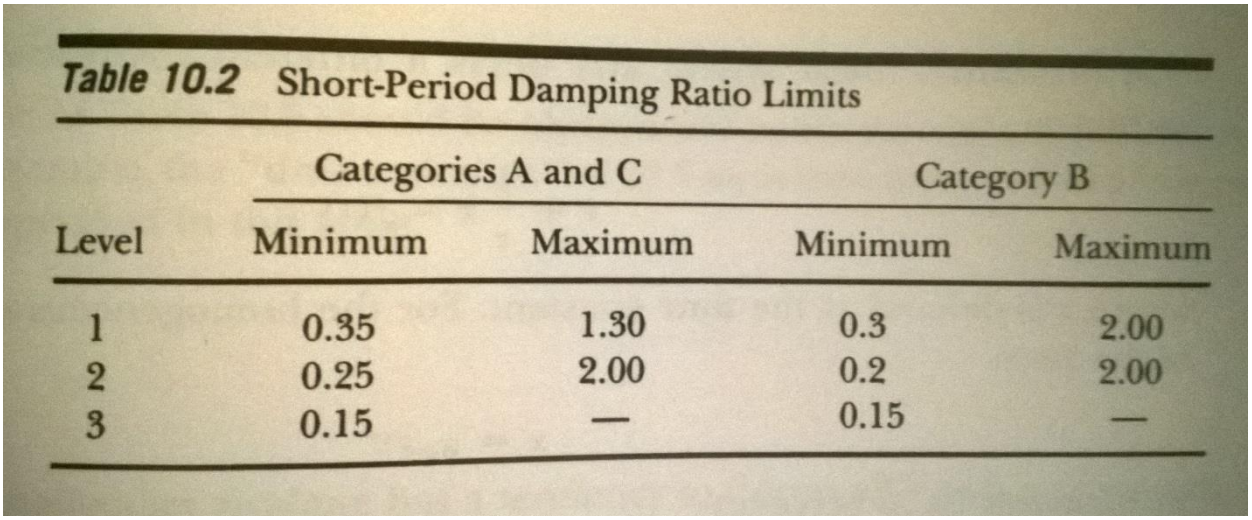

Table 10.2 Short-Period Damping Ratio Limits

	Categories A and C		Category B	
Level	Minimum	Maximum	Minimum	Maximum
1	0.35	1.30	0.3	2.00
2	0.25	2.00	0.2	2.00
3	0.15	—	0.15	—

Table XXX: short period mode flying quality

	short period mode damping quality	
	short period damping ratio	Flying quality level
Team 2 aircraft	0.74	1
MPX5 test case	0.69	1
Warrior test case	0.51	1

As seen in Table XXX, the damping ratio for the aircraft yields an acceptable level 1 flying quality.

Damping ratio and frequency target plot

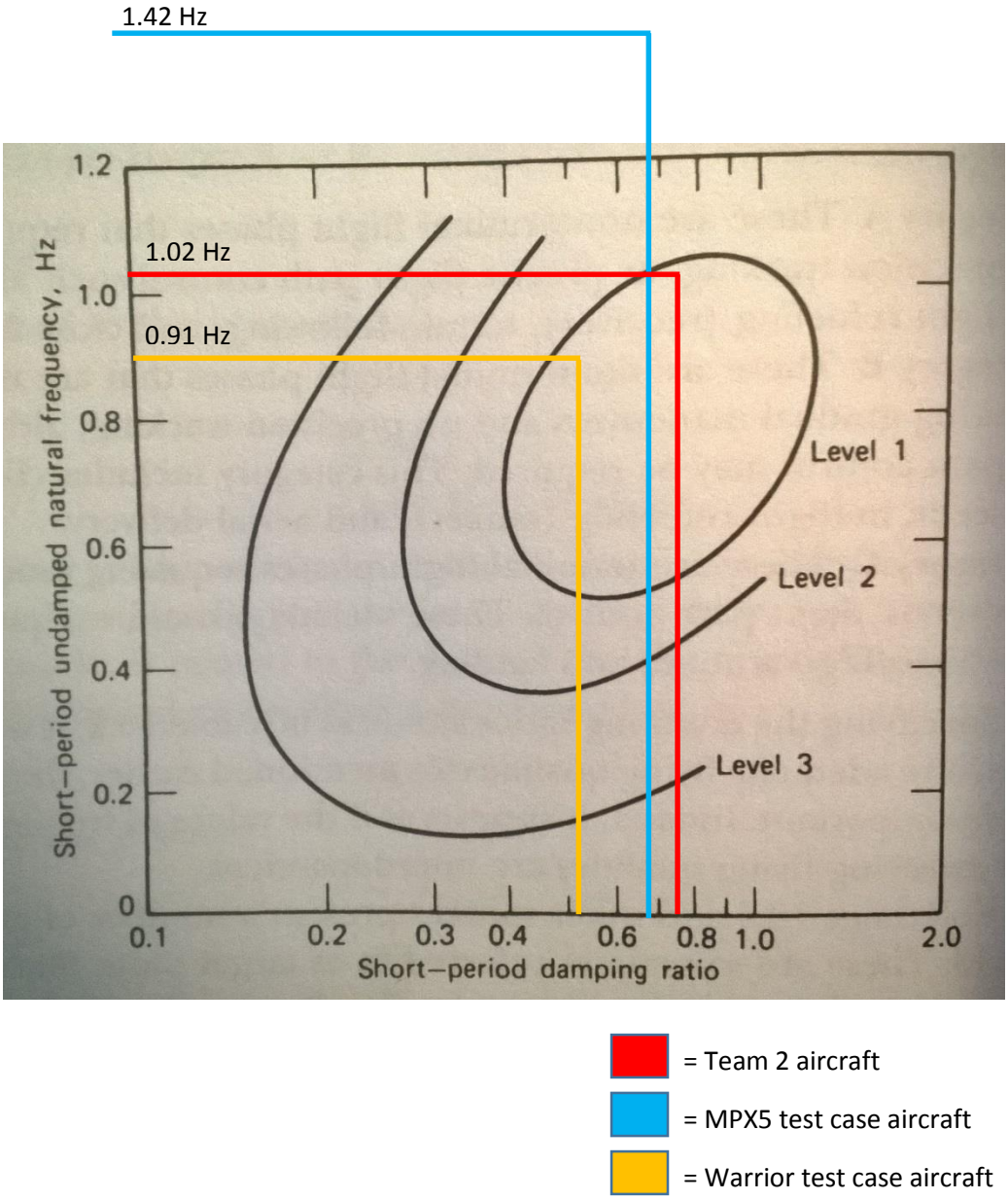

Figure XXX: target plot for short-period mode

Figure XXX illustrates the relationship between short-period frequency, damping ratio, and flying quality. Optimal flying quality depends on the coupled relationship between frequency and damping ratio.

Table XXX: short-period mode flying quality

	short period mode damping quality		
	short period damping ratio	natural frequency (Hz)	Flying quality level
Team 2 aircraft	0.74	1.02	1
MPX5 test case	0.69	1.42	3
Warrior test case	0.51	0.91	1

Table XXX illustrates that the coupled natural frequency and damping ratio yields an acceptable level 1 flying quality.

Roll mode

It is necessary for the aircraft to be capable of rolling quickly enough to accomplish the goals of specified phases of flight. The roll mode time constant can be used to characterize the time to roll. The following table correlates the time constant to levels of flying quality.

Table 10.3 Maximum Roll Mode Constant

Flight Phase Category	Class[a]	Level 1	Level 2	Level 3
A	I, IV	1.0	1.4	
	II, III	1.4	3.0	
B	All	1.4	3.0	10
C	I, II–C, IV	1.0	1.4	
	II–L, III	1.4	3.0	

[a] C and L refer to carrier and land operations.

$$\tau_{roll} = -\frac{1}{\sigma_{roll}}$$

$$where\ \tau_{roll} = roll\ mode\ time\ constant$$
$$\sigma_{roll} = roll\ mode\ root$$

Table XXX: roll mode flying quality

	roll mode time constant	
	Time constant (s)	Flying quality level
Team 2 aircraft	0.05	1
MPX5 test case	0.07	1
Warrior test case	0.09	1

Table XXX illustrates that the time constant for the current aircraft is very low. As such, the aircraft is able to roll quickly and be classified as level 1 flying quality for this flight mode.

Dutch roll mode

The dutch roll is characterized by a coupled and out-of-phase oscillation in the yaw and roll directions. The following figure illustrates an aircraft undergoing a dutch roll.

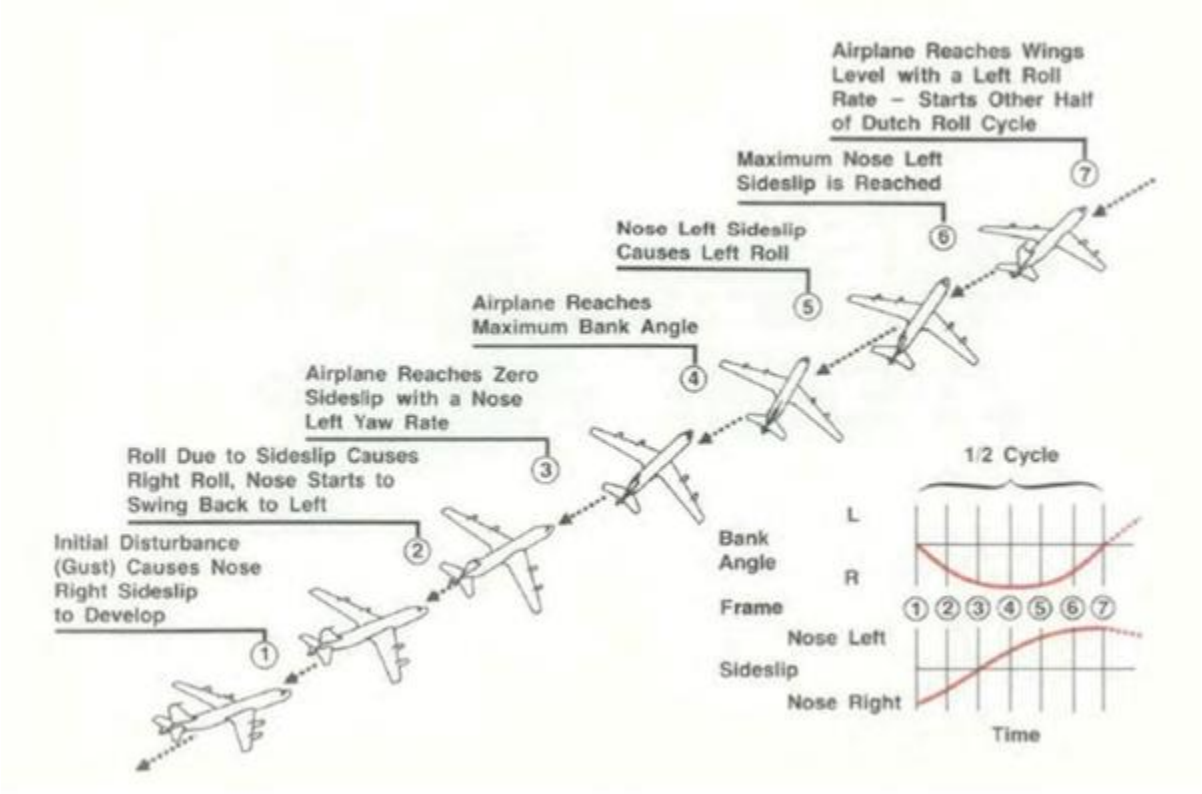

Figure XXX: illustration of dutch roll

The following figure correlates aircraft characteristics to flying quality.

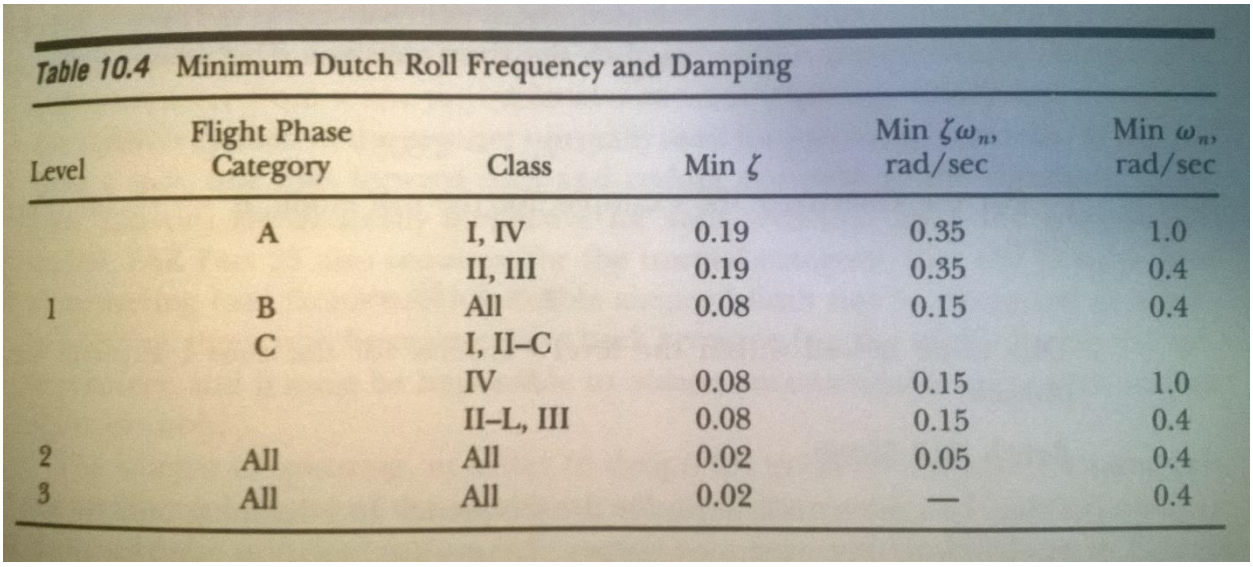

Table 10.4 Minimum Dutch Roll Frequency and Damping

Level	Flight Phase Category	Class	Min ζ	Min $\zeta\omega_n$, rad/sec	Min ω_n, rad/sec
	A	I, IV	0.19	0.35	1.0
		II, III	0.19	0.35	0.4
1	B	All	0.08	0.15	0.4
	C	I, II–C			
		IV	0.08	0.15	1.0
		II–L, III	0.08	0.15	0.4
2	All	All	0.02	0.05	0.4
3	All	All	0.02	—	0.4

Table XXX: dutch roll mode flying quality

	dutch roll mode			
	dutch roll damping ratio	damping ration * frequency (r/s)	dutch roll natural frequency (r/s)	Flying quality level
Team 2 aircraft	0.47	2.75	5.91	1
MPX5 test case	0.24	0.94	3.90	1
Warrior test case	0.19	0.50	2.64	1

As seen in Table XXX, the parameters for dutch roll frequency and damping ratio as well within bounds for level 1 flight quality.

Spiral mode

The spiral mode is characterized by the turning of the aircraft in the yaw direction over time. The following figure illustrates this motion.

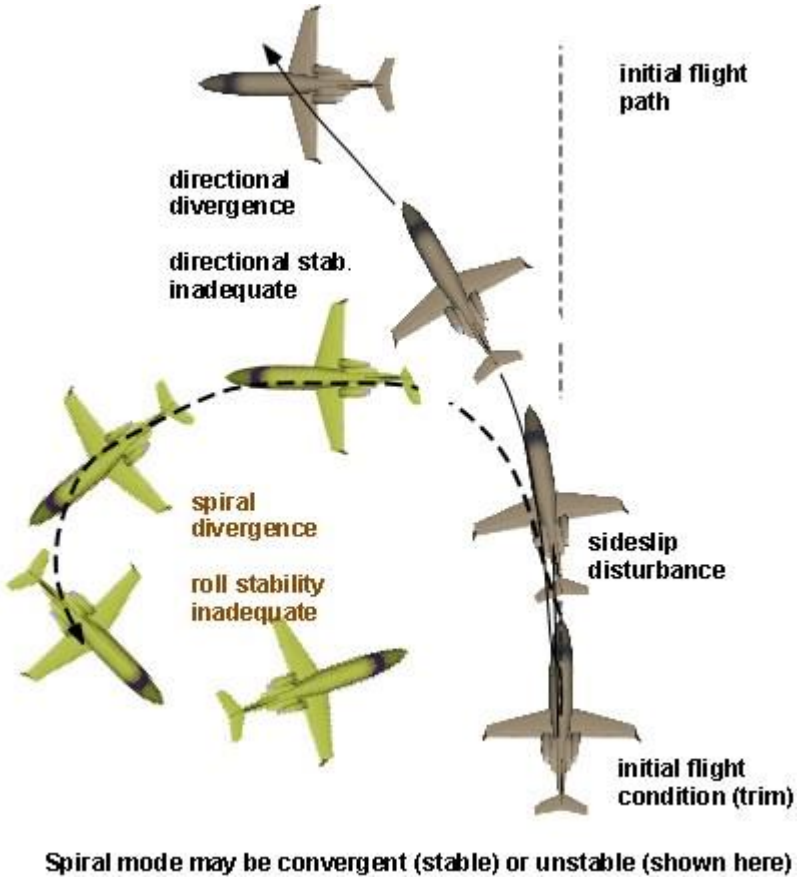

Figure XXX: illustration of spiral mode on aircraft yaw response

It is typical for the spiral mode of an aircraft to by divergent. More specifically, without pilot input, the yaw rate will continue to grow. It is desirable to keep the period for this motion very long such that the pilot can respond quickly enough to maintain the aircrafts intended flight path. The following table correlates the minimum time to double bank angle response to flying quality.

Table 10.5 Spiral Stability—Minimum Time-to-Double Amplitude

Class	Flight Phase Category	Level 1, sec	Level 2, sec	Level 3, sec
I and IV	A	12	12	4
	B and C	20	12	4
II and III	All	20	12	4

To determine time to double bank angle, the rudder was deflected for 1 degree for 1 second. The resulting time response was obtained from FlatEarth.

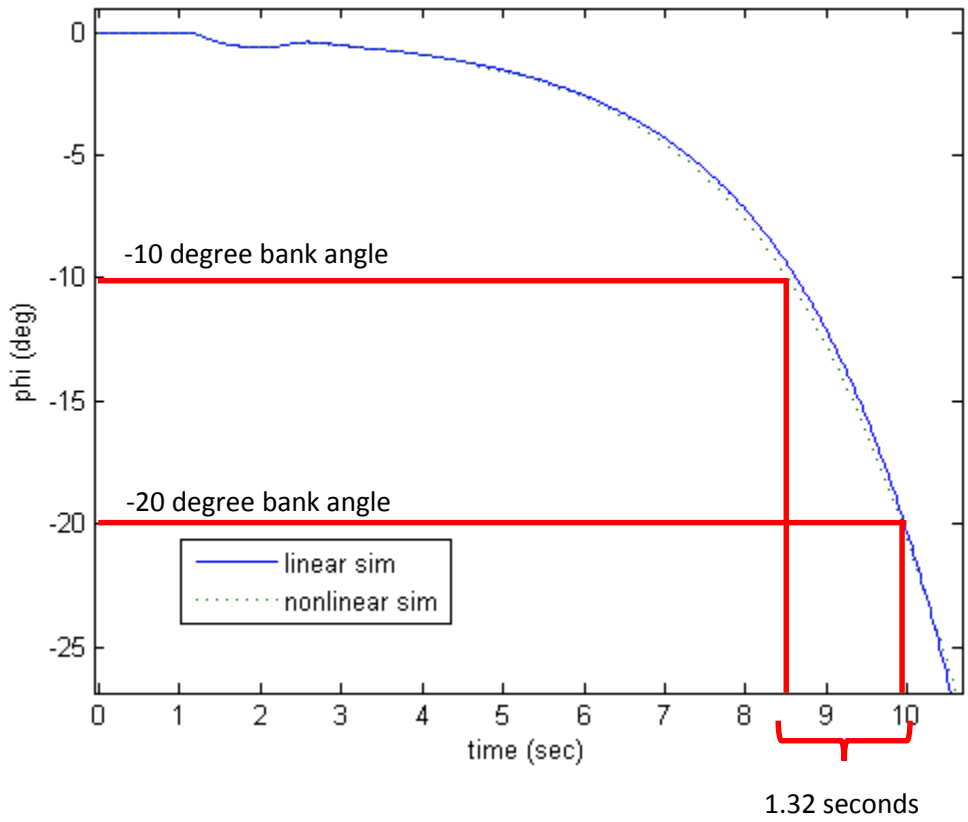

Figure XXX: determination of time to double bank angle

As seen, it takes approximately 1.32 seconds for the bank angle to double from 10 degrees to 20 degrees without pilot input. For comparison purposes, the same time response was obtained for the MPX5 and Warrior test case aircraft.

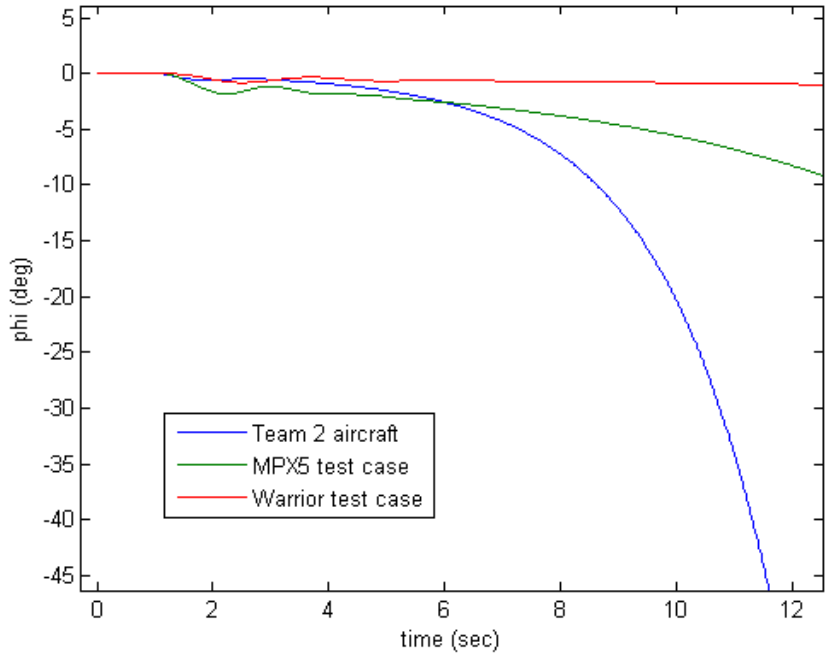

Figure XXX: comparison of spiral mode response for 3 aircraft

Table XXX: spiral mode flying quality

	spiral mode	
	time to double bank angle (s)	Flying quality level
Team 2 aircraft	1.32	3
MPX5 test case	3.50	3
Warrior test case	9.40	2.5

Table 3 shows that flying quality for the current aircraft in the spiral mode is very poor. As such, the pilot has to labor intensely to keep the aircraft from falling into a spiral dive.

Control feedback

From the open-loop flying quality analysis, we concluded that the aircraft displayed acceptable level 1 flying quality in every mode of flight except for in the spiral mode. Next, we will investigate how the use of a feedback control system can be utilized to improve spiral mode response.

From Table XXX, we see that the pole for spiral mode is 0.52 radians/s. A positive pole corresponds to an inherently unstable response. More specifically, the response can be improved by moving the pole towards the negative plane. This movement can be achieved through the use of proportional feedback controllers.

We recognize that the spiral mode pole can be found in 2 transfer functions: aileron input to roll rate output and rudder input to roll rate output. As such, applying feedback control to either the aileron or

rudder can move the pole. A root locus is used to identify the gains required to achieve this desired movement.

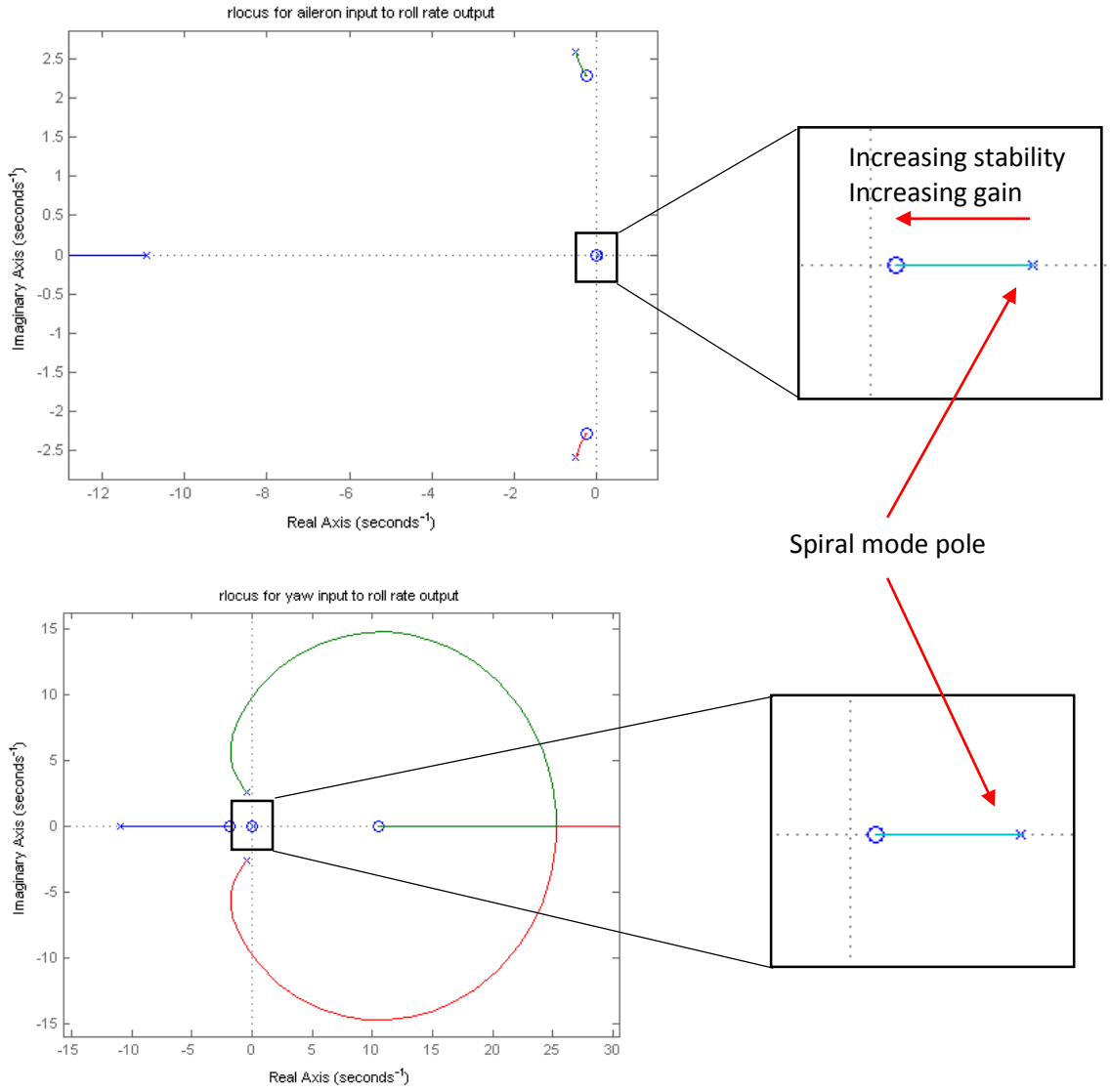

Figure XXX: root locus plots for aileron and rudder inputs to roll output

The following table illustrates the effect of various gain combinations on spiral mode response.

Table XXX: effect of closed-loop gain on spiral mode response

spiral mode closed-loop feedback response		
aileron gain	rudder gain	time to double bank angle (s)
0.10	-0.10	2.39
0.30	-0.30	2.59
0.30	-0.60	2.89
1.00	-1.00	3.79

From Table XXX, we see that as the gain values increase, the time to double bank angle also increases. This corresponds to a more desirable spiral mode response as the pilot is given more time to respond and correct bank angle. However, large values of gain result in sluggish aircraft performance as it takes longer for the aircraft to respond to pilot input.

Gain selection

Our team has chosen to utilize the following feedback control gains:

Table XXX: selection of feedback control gains

Feedback control gain selection	
aileron gain	1.00
rudder gain	-1.00
elevator gain	0

Table XXX shows that feedback control will not be utilized on elevator input. The open-loop flight quality analysis concluded that the aircraft displays acceptable level 1 flight quality in the longitudinal direction. As such, a feedback controller is not necessary.

The open-loop flight quality analysis for the lateral direction concluded that the aircraft displayed acceptable level 1 flying quality in every mode of flight except for in the spiral mode. As such, proportional feedback control was utilized to improve the spiral mode response by changing the time to double bank angle. However, moderate gains of -1 on the rudder and 1 on the aileron were only able to adjust time to double bank angle from 1.32 seconds to 3.79 seconds. Table XXX describes 3.79 seconds as a poor spiral mode response. Nonetheless, the MPX5 and the Warrior test case vehicles both display similarly low time to double bank angle values. Since these aircraft are both flight-worthy, it can be concluded that the flight quality correlation described in Table XXX does not properly apply to the smaller aircraft being analyzed by this report. With this notion, the feedback gains were selected by matching the spiral mode response of the aircraft to the spiral mode response of the MPX5 test case aircraft.

Simulator

A real-time controllable simulator was created for the purpose of test-flying the aircraft and for testing various feedback control inputs.

Operation

The following figure illustrates the graphical user interface (GUI) for the simulator.

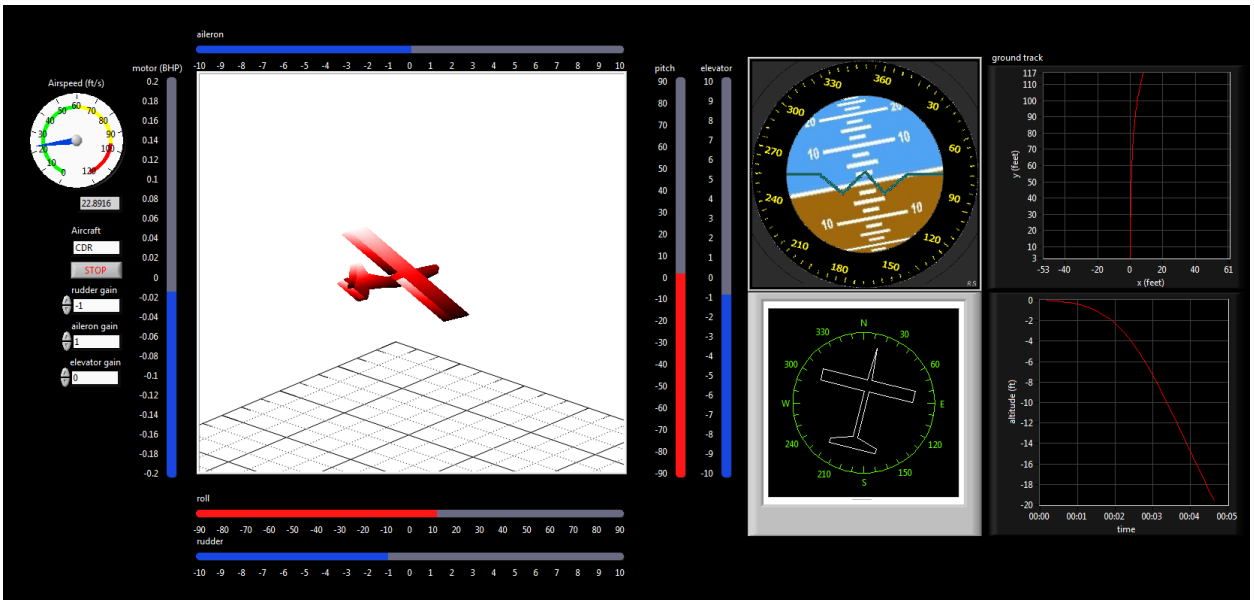

Figure XXX: graphical user interface for simulator

GUI display features

- 3-D render of aircraft
- Attitude gimbal display
- Heading display
- Ground track display
- Airspeed indicator
- Control surface input display
- Time plots of any state space variables or outputs

Control inputs

- Elevator
- Aileron
- Rudder
- Throttle

Simulator configuration parameters

- Specify aircraft
- Specify aileron proportional feedback gain
- Specify elevator proportional feedback gain

- Specify rudder proportional feedback gain
- Specify sim run-time rate

Control inputs are scanned from a joystick connected to the computer. The following figure illustrates the mapping of joystick axes to aircraft control surface input.

Where:
Y = elevator control
X = aileron control
RZ = rudder control
Throttle = motor power

Figure XXX: Joystick configuration for simulator control

Theory of operation

The following is a summary of the process for simulating the aircraft response in real-time:

1) FlatEarth v9.53 generates linearized state space for aircraft dynamics
2) MATLAB script exports state space to text config files
3) Labview 2014 reads config files on startup
4) Labview 2014 Control Design and Simulation Module utilized for performing state space calculations
5) Timing logic used to enforce real-time operation

The state space obtained from FlatEarth is illustrated in Figure XXX:

$$\dot{x} = \begin{bmatrix}
-0.274374 & 0 & 1.18648 & 0 & -4.42966 & 0 & 0 & -31.7607 & 0 & 0 & 0 & -2.24984E-5 \\
0 & -0.550251 & 0 & 4.48831 & 0 & -21.8603 & 31.7607 & 0 & 0 & 0 & 0 & 0 \\
-1.40187 & 0 & -4.80943 & 0 & 28.1478 & 0 & 0 & -4.92562 & 0 & 0 & 0 & 0.000939709 \\
0 & -0.372981 & 0 & -127.029 & 0 & 16.3327 & 0 & 0 & 0 & 0 & 0 & 0 \\
0.17384 & 0 & -0.605707 & 0 & -4.66447 & 0 & 0 & -0.00133912 & 0 & 0 & 0 & -3.56371E-5 \\
0 & 0.930556 & 0 & 9.98216 & 0 & -22.4291 & 0 & 0 & 0 & 0 & 0 & 0 \\
0 & 0 & 0 & 1 & 0 & 0.156224 & 0 & 0 & 0 & 0 & 0 & 0 \\
0 & 0 & 0 & 0 & 1 & 0 & 0 & 0 & 0 & 0 & 0 & 0 \\
0 & 0 & 0 & 0 & 0 & 1.01213 & 0 & 0 & 0 & 0 & 0 & 0 \\
0.988016 & 0 & 0.154352 & 0 & 0 & 0 & 0 & 1.53801E-10 & 0 & 0 & 0 & 0 \\
0 & 1 & 0 & 0 & 0 & 0 & -4.66915 & 0 & 30.25 & 0 & 0 & 0 \\
0.154352 & 0 & -0.988016 & 0 & 0 & 0 & 0 & 30.25 & 0 & 0 & 0 & 0
\end{bmatrix} x(t) + \begin{bmatrix}
0.218167 & 0 & 0 & 60.7851 & 0.0879502 & 0 & -1.21461 \\
0 & 0 & 7.08962 & 0 & 0 & 0.550251 & 0 \\
-6.95393 & 0 & 0 & 0 & 2.12726 & 0 & 4.53544 \\
0 & 107.268 & 6.9836 & 0 & 0 & 0.372981 & 0 \\
-35.2401 & 0 & 0 & 0.35162 & -0.078259 & 0 & 0.62528 \\
0 & -12.1626 & -19.2593 & 0 & 0 & -0.930556 & 0 \\
0 & 0 & 0 & 0 & 0 & 0 & 0 \\
0 & 0 & 0 & 0 & 0 & 0 & 0 \\
0 & 0 & 0 & 0 & 0 & 0 & 0 \\
0 & 0 & 0 & 0 & 0 & 0 & 0 \\
0 & 0 & 0 & 0 & 0 & 0 & 0 \\
0 & 0 & 0 & 0 & 0 & 0 & 0
\end{bmatrix} u(t)$$

$$y(t) = \begin{bmatrix}
1 & 0 & 0 & 0 & 0 & 0 & 0 & 0 & 0 & 0 & 0 & 0 \\
0 & 1 & 0 & 0 & 0 & 0 & 0 & 0 & 0 & 0 & 0 & 0 \\
0 & 0 & 1 & 0 & 0 & 0 & 0 & 0 & 0 & 0 & 0 & 0 \\
0 & 0 & 0 & 1 & 0 & 0 & 0 & 0 & 0 & 0 & 0 & 0 \\
0 & 0 & 0 & 0 & 1 & 0 & 0 & 0 & 0 & 0 & 0 & 0 \\
0 & 0 & 0 & 0 & 0 & 1 & 0 & 0 & 0 & 0 & 0 & 0 \\
0 & 0 & 0 & 0 & 0 & 0 & 1 & 0 & 0 & 0 & 0 & 0 \\
0 & 0 & 0 & 0 & 0 & 0 & 0 & 1 & 0 & 0 & 0 & 0 \\
0 & 0 & 0 & 0 & 0 & 0 & 0 & 0 & 1 & 0 & 0 & 0 \\
0 & 0 & 0 & 0 & 0 & 0 & 0 & 0 & 0 & 1 & 0 & 0 \\
0 & 0 & 0 & 0 & 0 & 0 & 0 & 0 & 0 & 0 & 1 & 0 \\
0 & 0 & 0 & 0 & 0 & 0 & 0 & 0 & 0 & 0 & 0 & 1 \\
0.988016 & 0 & 0.154352 & 0 & 0 & 0 & 0 & 0 & 0 & 0 & 0 & 0 \\
-0.00510254 & 0 & 0.0326617 & 0 & 0 & 0 & 0 & 0 & 0 & 0 & 0 & 0 \\
0 & 0.0330579 & 0 & 0 & 0 & 0 & 0 & 0 & 0 & 0 & 0 & 0 \\
0.00510254 & 0 & -0.0326617 & 0 & 0 & 0 & 0 & 1 & 0 & 0 & 0 & 0 \\
0.988016 & 0 & 0.154352 & 0 & 0 & 0 & 0 & 1.53801E-10 & 0 & 0 & 0 & 0 \\
0 & 1 & 0 & 0 & 0 & 0 & -4.66915 & 0 & 30.25 & 0 & 0 & 0 \\
0.154352 & 0 & -0.988016 & 0 & 0 & 0 & 0 & 30.25 & 0 & 0 & 0 & 0 \\
-0.274374 & 0 & 1.18648 & 0 & 0.23949 & 0 & 0 & 0 & 0 & 0 & 0 & -2.29727E-5 \\
0 & -0.550251 & 0 & -0.180838 & 0 & 0.937542 & 0 & 0 & 0 & 0 & 0 & 0 \\
-1.40187 & 0 & -4.80943 & 0 & -1.73966 & 0 & 0 & 0.0361652 & 0 & 0 & 0 & 0.000942745
\end{bmatrix} x(t) + \begin{bmatrix}
0 & 0 & 0 & 0 & 0 & 0 & 0 \\
0 & 0 & 0 & 0 & 0 & 0 & 0 \\
0 & 0 & 0 & 0 & 0 & 0 & 0 \\
0 & 0 & 0 & 0 & 0 & 0 & 0 \\
0 & 0 & 0 & 0 & 0 & 0 & 0 \\
0 & 0 & 0 & 0 & 0 & 0 & 0 \\
0 & 0 & 0 & 0 & 0 & 0 & 0 \\
0 & 0 & 0 & 0 & 0 & 0 & 0 \\
0 & 0 & 0 & 0 & 0 & 0 & 0 \\
0 & 0 & 0 & 0 & 0 & 0 & 0 \\
0 & 0 & 0 & 0 & 0 & 0 & 0 \\
0 & 0 & 0 & 0 & 0 & 0 & 0 \\
0 & 0 & 0 & 0 & -1 & 0 & 0 \\
0 & 0 & 0 & 0 & 0 & 0 & -0.0330579 \\
0 & 0 & 0 & 0 & 0 & -0.0330579 & 0 \\
0 & 0 & 0 & 0 & 0 & 0 & 0.0330579 \\
0 & 0 & 0 & 0 & 0 & 0 & 0 \\
0 & 0 & 0 & 0 & 0 & 0 & 0 \\
0 & 0 & 0 & 0 & 0 & 0 & 0 \\
0.218167 & 0 & 0 & 60.7851 & 0.0879502 & 0 & -1.21461 \\
0 & 0 & 7.08962 & 0 & 0 & 0.550251 & 0 \\
-6.95393 & 0 & 0 & 0 & 2.12726 & 0 & 4.53544
\end{bmatrix} u(t)$$

Figure XXX: FlatEarth state space output to Labview

State Space feedback control

It is desired to be able to apply proportional feedback control gains to the aileron, rudder, and elevator for aircraft testing. The figure below illustrates how the open-loop state space is wrapped by a proportional controller.

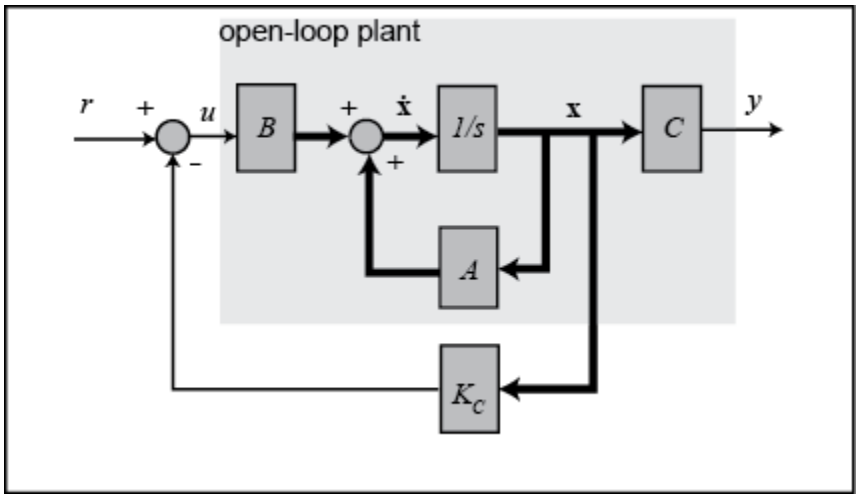

Figure XXX: proportional feedback controller applied to state space

With the addition of the proportional controller, the state space equation can then be written as:

$$\dot{x} = (A - B * K_c)x + Br$$
$$y = Cx + Bd$$

$$where\ x = state\ variables$$
$$r = input$$
$$K_c = proportional\ feedback\ constant$$

Simulator validation

Longitudinal Direction

The longitudinal model was tested by injecting a doublet input on the elevator. More specifically, the elevator was deflected 1 degree from trim for 1 second, then deflected -1 degrees from trim for 1 second, and then brought back to trim. The following figures show the FlatEarth output and Labview simulation output.

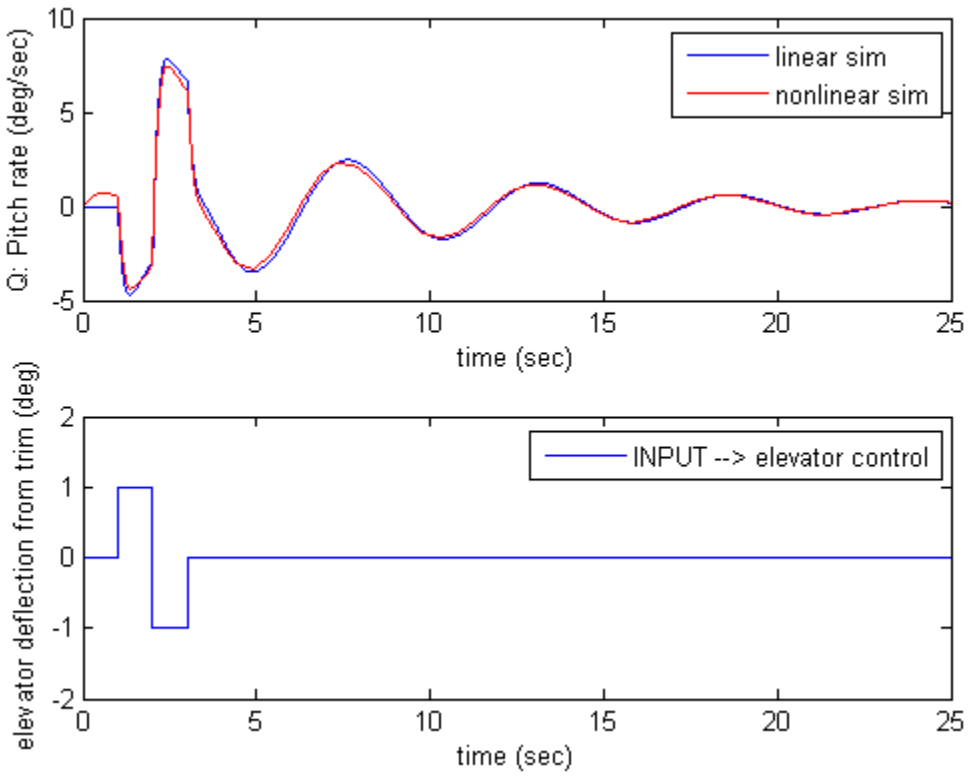

Figure XXX: FlatEarth - pitch rate response to doublet elevator input

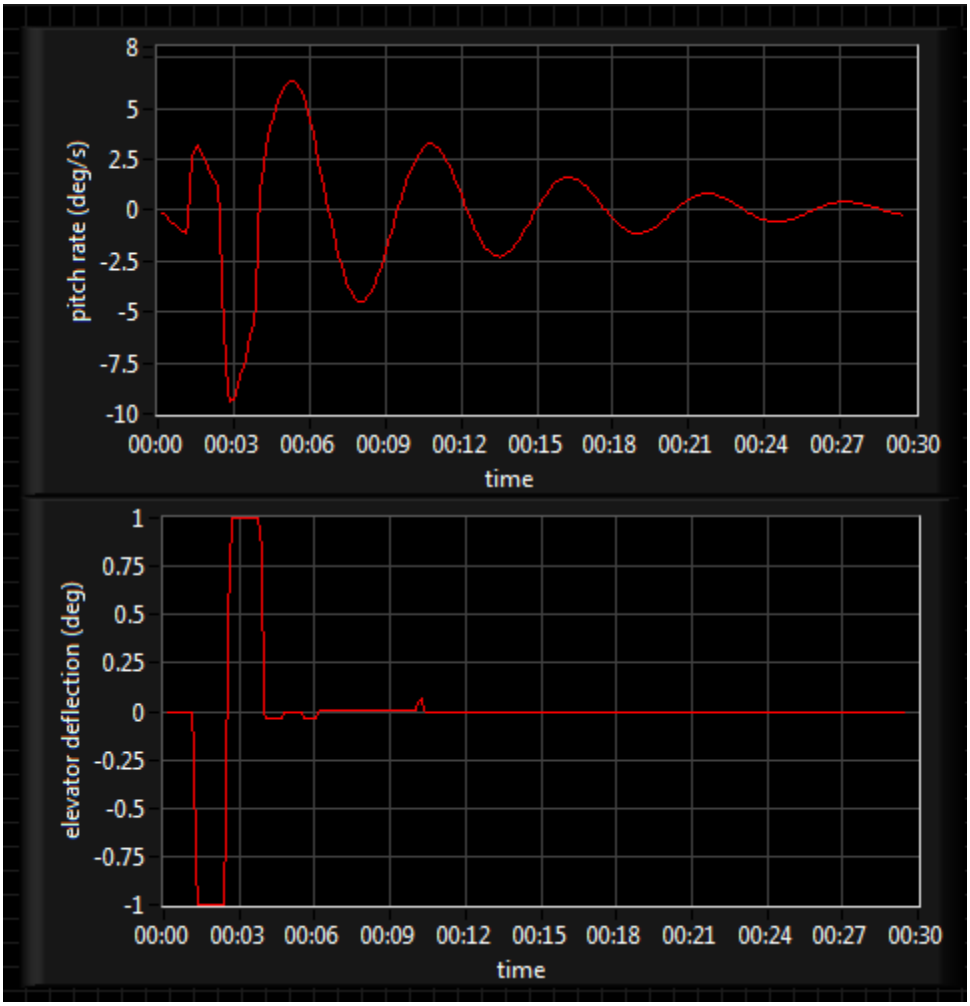

Figure XXX: Labview simulation – pitch rate response to doublet elevator input

We see that the nonlinear FlatEarth, linear FlatEarth, and Labview simulation results are all in acceptable agreement. As such, the following can be concluded:

- Linearized model acceptable for near-trim flight
- Labview simulation model acceptably operating at real-time

We also see that with an elevator deflection, the pitch rate dampens out and approaches a steady state value of zero. This corresponds to a dynamically stable aircraft in the longitudinal direction. This observation is in agreement with the flight qualities analysis.

References

[1] Roskam, Jan, “Airplane Design”

[2] Raymer, Daniel, “Aircraft Design”

[3] Roskam, Jan, “Methods for Estimating Stability and Control Derivatives of Conventional Subsonic Airplanes”

[4] McCormick, Barnes, “Aerodynamics Aeronautics and Flight Mechanics”

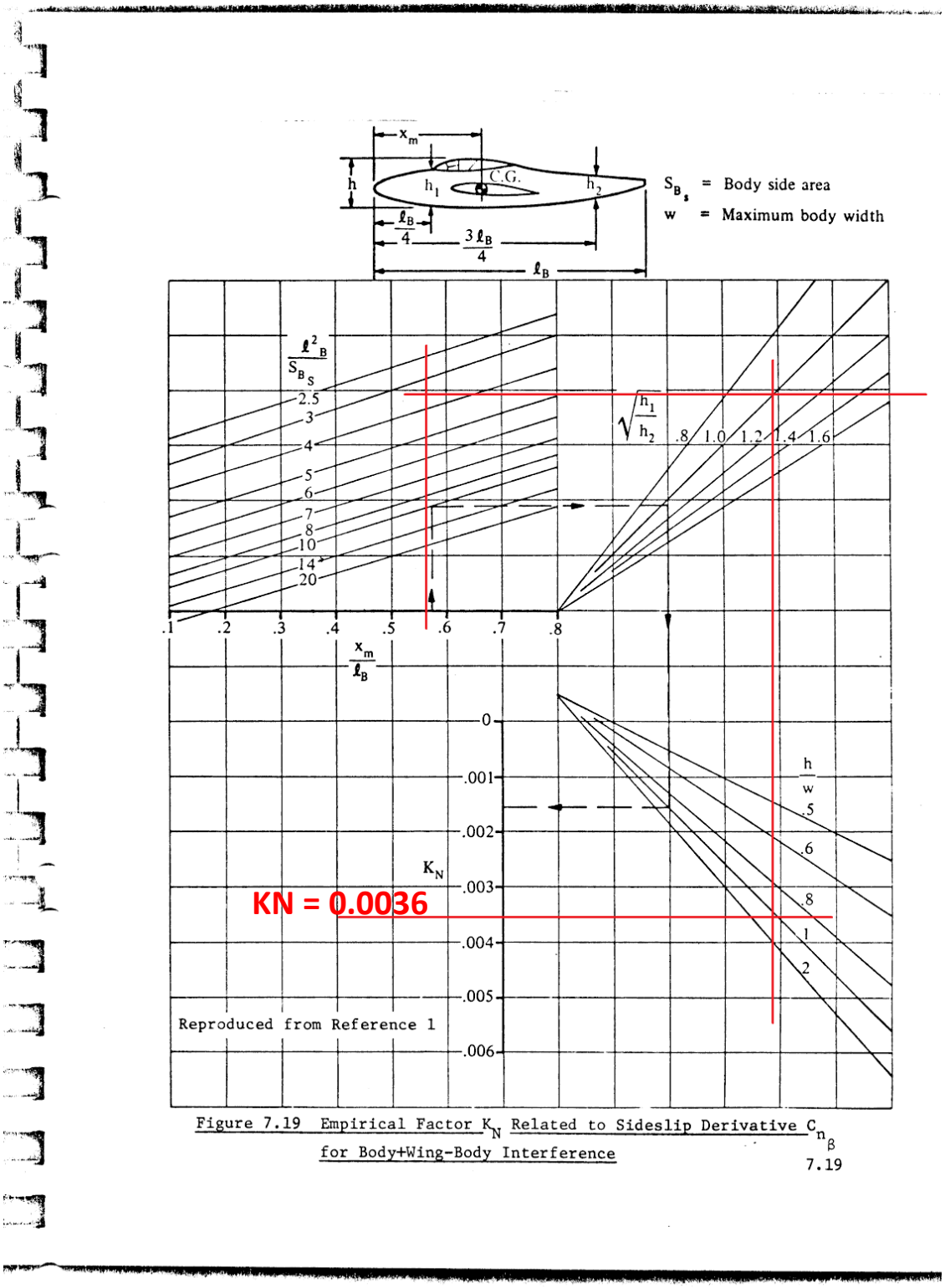

Figure 7.19 Empirical Factor K_N Related to Sideslip Derivative C_{n_β} for Body+Wing-Body Interference

7.19

Figure A1: Determination of KN for vertical tail X-plots [3]

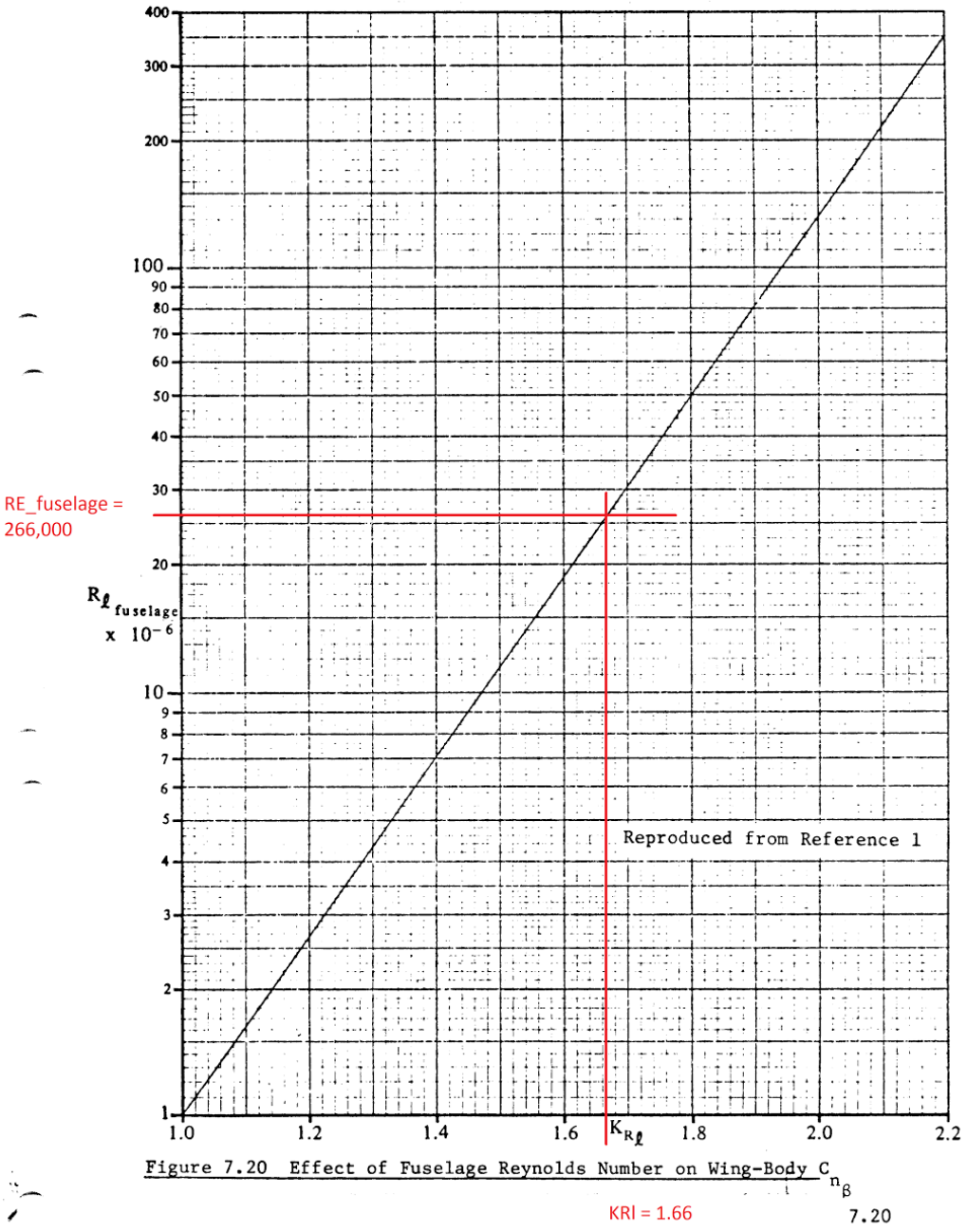

Figure A2: Determination of KRl for vertical tail X-plots [3]

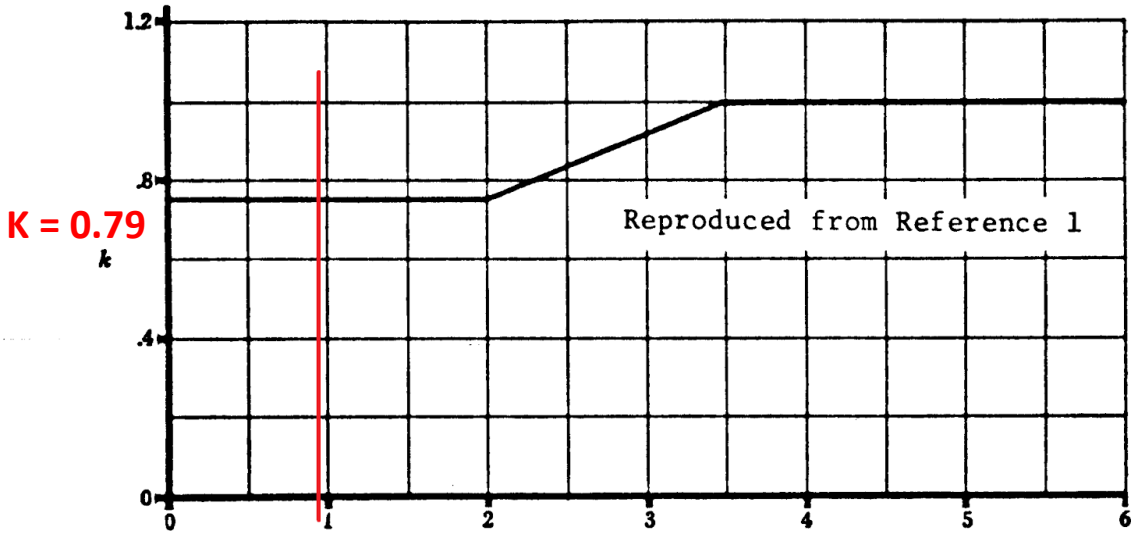

(For definition of $2r_1$ see Figure 7.10)

Figure 7.3 Empirical Factor for Estimating the Sideslip Derivative $C_{y_{\beta_v}}$ for Single Vertical Tails

Figure A3: Determination of k for vertical tail X-plots [3]